CHEMISTRY OF MATERIALS

pubs.acs.org/cm

Article

Direct CVD Growth of a Graphene/MoS_2 Heterostructure with Interfacial Bonding for Two-Dimensional Electronics

Eunho Lee, Seung Goo Lee, Wi Hyoung Lee, Hyo Chan Lee, Nguyen Ngan Nguyen, Min Seok Yoo, and Kilwon Cho*

Cite This: https://dx.doi.org/10.1021/acs.chemmater.0c00503

Read Online

ACCESS | Metrics & More | Article Recommendations | Supporting Information

ABSTRACT: This article describes a novel method for the direct synthesis of patterned graphene on transition-metal dichalcogenides (TMDs) such as molybdenum disulfide (MoS_2) with chemical vapor deposition (CVD) that uses a UV/ozone-treated solid carbon source, 1,2,3,4-tetraphenylnaphthalene (TPN) as the graphene growth precursor. The UV/ozone treatment of the TPN film on the MoS_2 layer improves the interfacial adhesion between the TPN and MoS_2 layers. The surface-adhered TPN is directly converted to graphene on the MoS_2 layer, which results in a sharp interface between graphene and MoS_2. The graphene/MoS_2 heterostructure with interfacial bonding yields excellent electrical and mechanical characteristics that facilitate charge injection by reducing contact resistance and improving bending stability. The excellent contact enhances the field-effect mobility of MoS_2 field-effect transistors to values up to three times higher than that of the devices using source-drain electrodes prepared with the conventionally transferred CVD-grown graphene. The proposed method for the direct synthesis of graphene on TMDs is expected to have wide applications in nanoelectronics based on 2D materials.

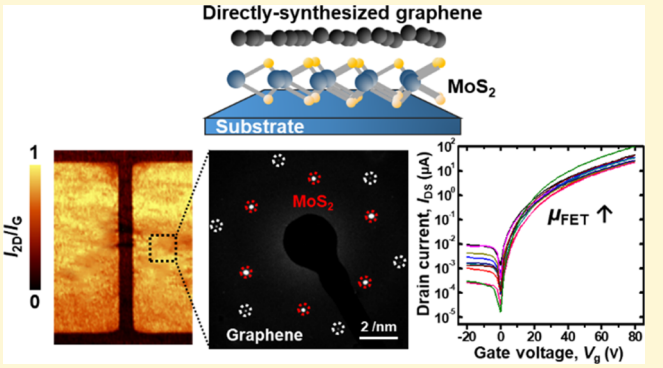

1. INTRODUCTION

Two-dimensional transition metal dichalcogenides (TMDs) have received much attention because of their unique electronic and optical properties.[1−7] In particular, a monolayer of molybdenum disulfide (MoS_2) has a large direct band gap (1.9 eV), in contrast to graphene, and thus has been widely investigated for the semiconducting layer in electronic devices.[8−10] For example, field-effect transistors (FETs) based on MoS_2 monolayers exhibited a large on/off current ratio (I_{on}/I_{off}) and high charge carrier mobility (μ) and are regarded as one of the leading candidates for use in next-generation ultrathin semiconductors.[11−13]

Further optimization of the MoS_2 FETs requires the fundamental understanding of the characteristics of MoS_2 and metal source/drain electrodes. Charge transport in ultrathin electronic devices is largely dominated by their contact properties due to their large surface-to-volume ratio and lack of surface chemical bonds. Therefore, in order to achieve high electrical properties, the characteristics of the interfaces between MoS_2 and metal electrodes must be studied. Theoretically, the Schottky barrier height, φ_B, for electrons can be reduced to zero using metals that have a low work function (WF) and a strong interaction according to the Schottky−Mott rule.[14,15] However, there are no dangling bonds on the surfaces of MoS_2 layers, so the interaction between such layers and metals is relatively weak.[16,17] This feature of the MoS_2−metal interaction results in the formation of midgap or defect-induced energy gap states of MoS_2 that increase the contact resistance, R_C, and produce a high Schottky barrier, φ_B.[18] For this reason, high-performance MoS_2-based devices are still being studied.

To achieve MoS_2-based electronic devices with a high μ, several studies have attempted to engineer the MoS_2/electrode interface to optimize the contact of the electrode with the MoS_2 layer. For example, the use of metals such as Ni, Ti/Au, and Sc can substantially reduce the contact resistance and as a consequence improve the electrical characteristics of the fabricated devices.[19−21] To improve on this approach, the transformation of the phase of the MoS_2 layer to reduce contact resistance has been attempted;[22] the conversion of the MoS_2 layer from the semiconducting 2H phase to the metallic 1T phase successfully decreases contact resistance. However, the metal deposition method used in such studies results in inhomogeneities at the MoS_2−metal interface.[23] This unstable interface decreases electron injection efficiency and results in

Received: February 6, 2020
Revised: May 5, 2020
Published: May 6, 2020

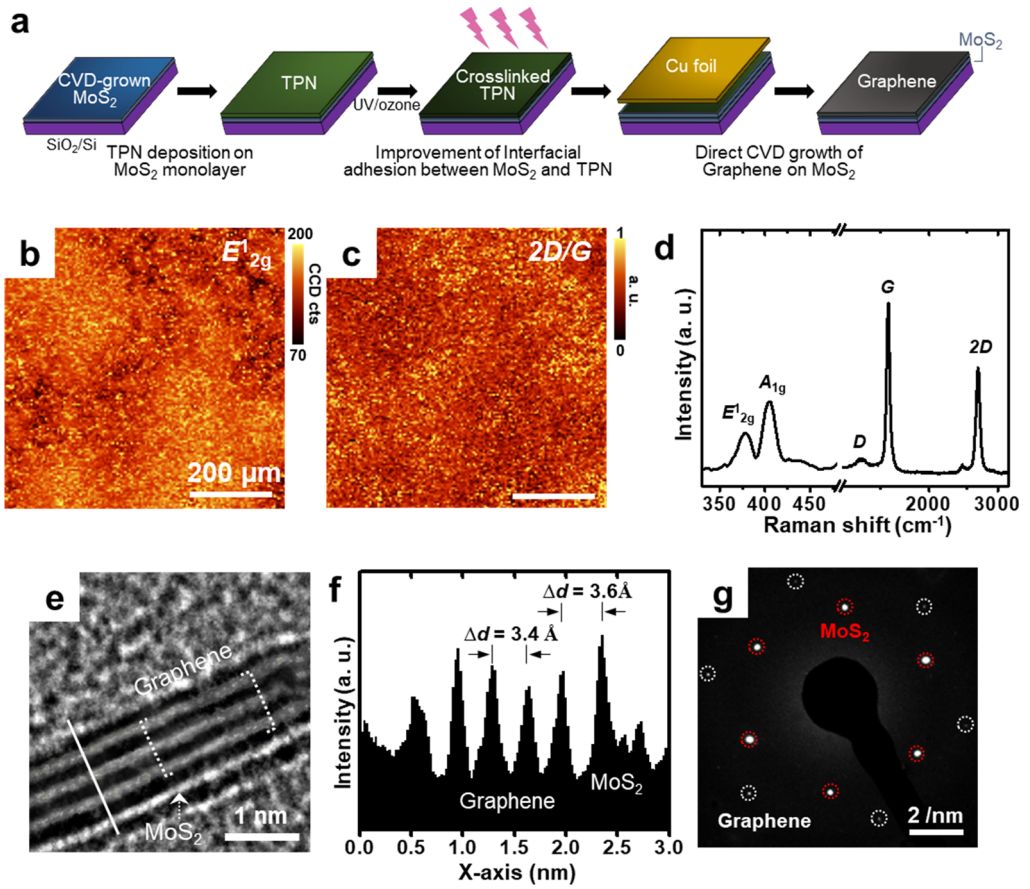

Figure 1. Synthesis and characterization of graphene/MoS_2 heterostructure. (a) Schematic diagram of the direct synthesis of graphene/MoS_2 heterostructure on SiO_2/Si substrate. (b) E_{2g}^1 and (c) 2D/G Raman mapping data of synthesized graphene/MoS_2 heterostructure. (d) Average single Raman spectrum from 100 points within the synthesized graphene/MoS_2 heterostructure. (e) High-resolution cross-sectional TEM image of the synthesized graphene/MoS_2 (f) Depth-profile of solid white line. (g) Hexagonal SAED pattern images from synthesized graphene (white circle) and MoS_2 monolayer (red circle) on lacey carbon TEM grid.

an increase in the contact resistance. In addition, atomically thin layers of MoS_2 can be damaged by metal adatoms during the metal deposition process. To solve these problems, the use of other electrodes has been widely studied, with special attention to graphene because of its extraordinary electrical properties.[24−27] The μ and I_{on}/I_{off} are usually higher in MoS_2-FETs that use graphene electrodes than in devices that use conventional metal electrodes. The use of graphene electrodes in MoS_2-FET devices has the advantages of an easily-tunable work function, high conductivity, and an undamaged MoS_2 layer. However, the process of transferring graphene to the MoS_2 layer can introduce interfacial contamination that degrades the electrical characteristics of the devices. Therefore, a method for the direct synthesis of graphene on the MoS_2 layer which eliminates this transfer process is required for the fabrication of high-performance electronic devices.

Here, we propose a new method for the patterned growth of high-quality CVD graphene directly onto an MoS_2 layer in which a solid carbon source [1,2,3,4-tetraphenylnaphthalene (TPN)] on the MoS_2 layer is selectively exposed to UV/ozone. The UV/ozone treatment of the solid carbon source increases the interfacial adhesion between TPN and the MoS_2 layer. This strengthened interfacial adhesion yields conformal contact at the interface between TPN and the MoS_2 layer. As a result, patterned graphene can be grown directly on the MoS_2 layer with the assistance of Cu vapor, which enhances the electrical characteristics of the resulting MoS_2-FET because of the efficient charge injection through the improved interface. Our proposed method minimizes the contact resistance, R_C, so the measured μ of the resulting MoS_2-FETs is more than tripled. Furthermore, the measured φ_B between graphene and MoS_2 was found to be almost zero with ohmic contact under back-gate modulation. This graphene growth process produces enhanced interfacial adhesion and can thus provide a method for the engineering of the contacts and interfaces between two-dimensional layers in atomically thin electronics.

2. EXPERIMENTAL SECTION

2.1. Graphene/MoS_2 Heterostructure CVD Synthesis. The mixed precursors (MoO_3 3.5 mg, NaCl 1.5 mg) for MoS_2 growth were placed in the center of a quartz boat, and the prepared SiO_2/Si substrate was placed on the quartz boat. An aluminum oxide crucible containing sulfur (S) powder for the sulfurization of MoO_3 was placed 17 cm above the quartz boat. The quartz boat and crucible were loaded into the quartz tube; it was evacuated, and then the prepared substrate was heated to a growth temperature (T = 730 °C) under the pressure P = 150 Torr. Simultaneously, the heater located at the crucible containing S was also heated to T = 200 °C. Then, graphene was synthesized on the MoS_2 layer where it forms a vertical heterostructure. TPN was spin-coated onto the MoS_2-grown SiO_2/Si substrate. The TPN film was exposed to UV/ozone in the ambient atmosphere for 7 min. Then, a Cu foil was placed on the prepared substrate, and they were loaded into a quartz tube that was

https://dx.doi.org/10.1021/acs.chemmater.0c00503
Chem. Mater. XXXX, XXX, XXX−XXX

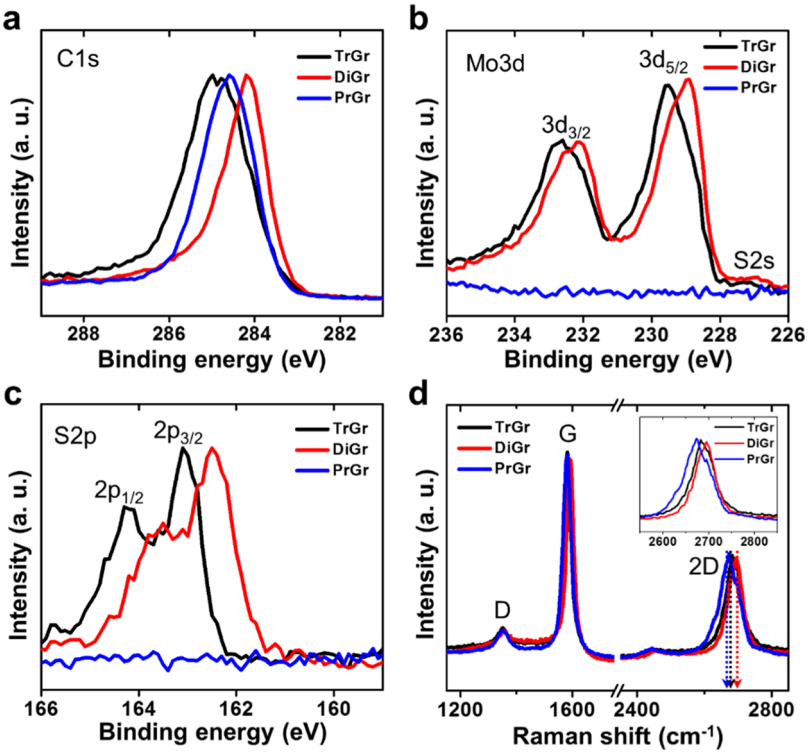

Figure 2. XPS analysis of interfacial chemistry. (a) C 1s, (b) Mo 3d, and (c) S 2p XPS analysis of the peak at the interface between MoS_2 monolayer and graphene synthesized using different methods. (d) Single Raman spectrum of different graphene on MoS_2 monolayer.

subsequently evacuated. The sample was then heated to T = 900 °C with 100 sccm Ar gas (pressure $P = 2.7 \times 10^{-2}$ Torr) to synthesize graphene.

2.2. Device Fabrication and Electrical *I*–*V* Measurement. The MoS_2 monolayer was grown with CVD on the SiO_2/Si substrate; then, TPN as the graphene growth precursor was spin-coated onto the MoS_2 monolayer. To pattern the graphene S/D electrodes, the precursor was selectively exposed to UV/ozone through a shadow mask. The TPN in the UV/ozone-exposed region adhered to the MoS_2 monolayer, so a graphene/MoS_2 vertical structure was prepared on the SiO_2/Si substrate. The selective UV/ozone exposure yielded a patterned graphene structure in the MoS_2-FET device on the SiO_2/Si substrate. Finally, the electrical characteristics of the fabricated devices were characterized at room temperature in a dark environment using a Keithley 2636A instrument under vacuum (10^{-3} Torr).

3. RESULTS AND DISCUSSION

SiO_2/Si substrate was sequentially rinsed with ethanol, acetone, isopropyl alcohol, and DI water to remove all organic contaminants from its surface. Then, a MoS_2 monolayer was synthesized on the SiO_2/Si substrate using the molten-salt-assisted CVD method in a quartz tube (Figure S1).[28] The synthesized MoS_2 was found to be a monolayer, and its characteristics were confirmed with atomic force microscopy (AFM) and Raman spectroscopy (Figure S2). After the growth of MoS_2 had finished, TPN was spin-coated onto the MoS_2/SiO_2/Si substrate (Figure 1a) to a thickness of ∼30 nm. The TPN film was exposed to UV/ozone in the ambient atmosphere for 7 min; this treatment increases the interfacial adhesion between the TPN film and the MoS_2 layer.[29] The effects of UV/ozone exposure to the TPN film on the MoS_2 layer are discussed below. Then, a Cu foil was placed on the prepared substrate to supply Cu vapor as the catalyst for graphene growth.

The synthesis of the graphene/MoS_2 heterostructure was confirmed by examining the two-dimensional Raman mapping of the intensity of the E_{2g}^1 peak (382.1 cm^{-1}) and determining the ratio of the intensity, I_{2D} of the 2D peak (2694 cm^{-1}) to the intensity, I_G of the G-peak (1589 cm^{-1}) over a 700 μm × 700 μm area on the SiO_2/Si substrate (Figure 1b,c). The E_{2g}^1 peak is a characteristic Raman peak of MoS_2 layers, and the 2D peak and G peak are characteristic Raman peaks of graphene. These two-dimensional Raman mappings indicate that a large-area vertical graphene/MoS_2 heterostructure has been uniformly synthesized. The measured single Raman spectrum also clearly shows the characteristic E_{2g}^1 peak (382.14 cm^{-1}) and the A_{1g} peak (401.6 cm^{-1}) of MoS_2, and the D peak (1382 cm^{-1}), G peak (1589 cm^{-1}), and 2D peak (2694 cm^{-1}) of graphene grown from UV/ozone-treated TPN (Figure 1d). The 2D peak has a full width at half maximum = 67 cm^{-1}, which suggests that the graphene synthesized on MoS_2 is approximately four layers thick.[30] In addition, during the graphene growth process, the TPN and grown graphene on MoS_2 might prevent generation of defects in MoS_2. This can be seen through the analysis of photoluminescence (PL), and it was seen that graphene acted as a passivation layer, considering that there was almost no change in the measured PL spectra before and after graphene growth (Figure S3). These results were confirmed by inspecting a cross-sectional transmission electron microscopy (TEM) image (Figure 1e). This TEM image shows that layer-structured graphene has been successfully prepared on the MoS_2 monolayer, and that the interface between graphene and MoS_2 is sharp. The measured interlayer distance (Δd) in the graphene structure is 3.4 Å, which is similar with the results of previous studies, and the graphene and MoS_2 layers are separated by an interlayer distance of 3.6 Å, which is also consistent with the previous results (Figure 1f).[31] Even though the interaction between

https://dx.doi.org/10.1021/acs.chemmater.0c00503
Chem. Mater. XXXX, XXX, XXX−XXX

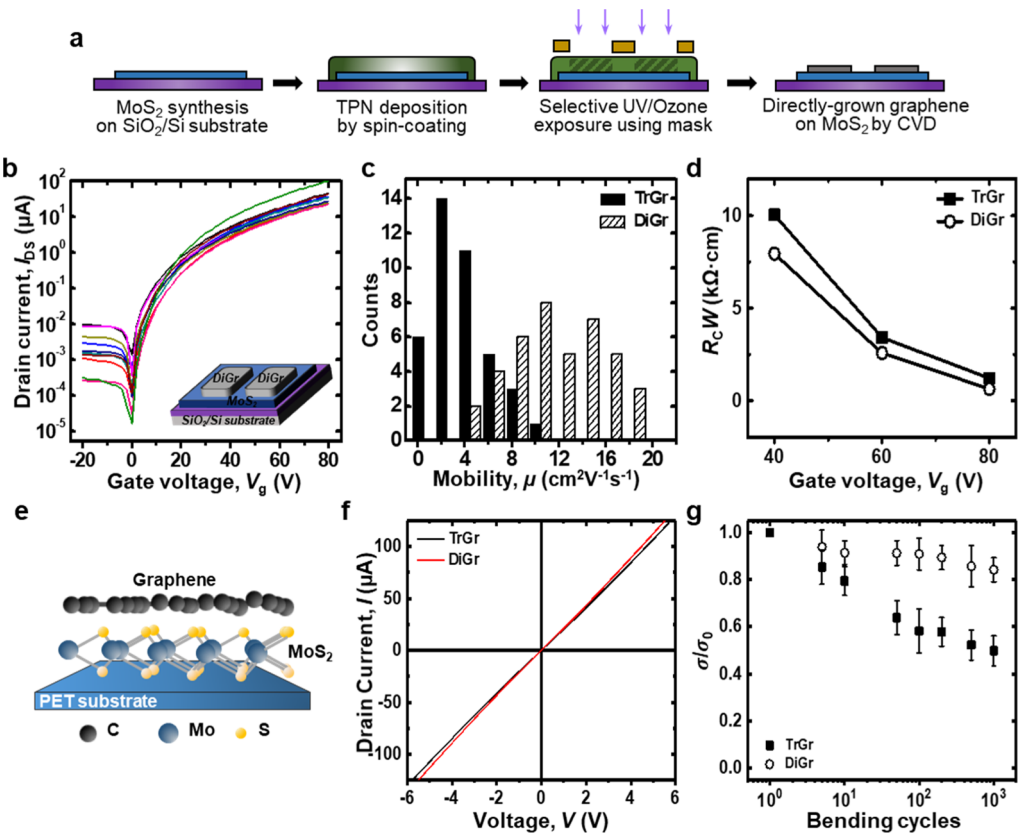

Figure 3. Electrical characteristics and bending stability of graphene/MoS_2 heterostructure. (a) Schematic diagram of the MoS_2-FETs fabrication process using DiGr as S/D electrodes on SiO_2/Si substrate. (b) 10 representatives of transfer curves of the fabricated MoS_2-FETs based on DiGr electrodes. (inset) Device structure scheme of the fabricated MoS_2-FET devices. (c) Statistics diagram of the measured electron mobilities from total 40 fabricated MoS_2-FETs using TrGr and DiGr electrodes. (d) Comparison of normalized contact resistance between TrGr and DiGr electrode-based devices at different gate voltages. (e) Schematic diagram of the transferred graphene/MoS_2 on PET substrate. (f) Measured electrical $I-V$ curves of MoS_2 2-terminal devices using TrGr (black) and DiGr (red) electrodes. (g) Conductance changes under repeated bending cycles to bending radius 10 R of MoS_2 2-terminal devices using TrGr and DiGr electrodes.

graphene and MoS_2 is enhanced by interfacial adhesion bonding, the interfacial adhesion bonding is not fully formed on the entire surface.[29,32] It might not be strong enough to reduce the interlayer distance. The weak interaction between graphene and MoS_2 is probably the reason that the interlayer distance between graphene/MoS_2 is slightly larger than the graphene−graphene interlayer distance.

The SAED pattern of the graphene/MoS_2 heterostructure contains diffraction spots due to both MoS_2 (red circles) and graphene (white circles) (Figure 1g). These diffraction patterns confirm the (100) lattice spacing of the graphene and MoS_2 layers.[33] The surface morphology of the synthesized graphene/MoS_2 heterostructure is very clean, and there are no undesirable residues on the graphene surface (Figure S4). Therefore, this heterostructure is appropriate for surface-sensitive ultrathin electronic device applications.

To quantify the effects of the growth of graphene on the MoS_2 monolayer, we prepared three different samples; one is directly grown graphene (DiGr) on a MoS_2 monolayer using our proposed method, the other is a CVD-grown graphene conventionally transferred to a MoS_2 (TrGr) and another is directly grown graphene on a pristine SiO_2/Si substrate (PrGr) to exclude any effects of the MoS_2 monolayer on the growth of graphene.[29] The TrGr sample was CVD-grown from methane (CH_4) and transferred to the MoS_2 monolayer using poly(methyl methacrylate) (PMMA) as a supporting layer. The PMMA/graphene film was transferred to the MoS_2 monolayer on the SiO_2/Si substrate using the conventional method, then rinsed in acetone to remove the PMMA. PrGr was prepared on a SiO_2/Si substrate with the same method.

The changes in the interfacial chemistry during UV/ozone exposure were confirmed by analyzing X-ray photoelectron spectroscopy (XPS) depth-profile spectra of the three graphene samples (TrGr, DiGr, PrGr) at the interface between TPN and MoS_2 (Figure 2a). The peaks in the C 1s XPS analyses for TrGr/MoS_2 and DiGr/MoS_2 are clearly shifted when compared to those of PrGr. The peaks for TrGr are blue-shifted, which is probably due to the various functional groups (e.g., carbonyl, carboxyl) that are coming from the PMMA residues during the graphene transfer process.[34] The deconvolution of the C 1s XPS results for TrGr indicates that the ratio of the intensities of the O−C═O peak (288.3 eV) and the C−O (286.2 eV) peak is higher than that for PrGr (Figure S5). In contrast, there are no peaks due to PMMA residues in the C 1s spectrum of DiGr because no transfer procedure was used. Instead, the spectrum contains new peaks at low binding energies (283.3 and 284.1 eV), which are due to Mo−C and S−C bonds at the interface between DiGr and MoS_2.[35,36] This interfacial bonding is likely to be the result of a penetrated ozone-mediated reaction during the UV/ozone exposure; this phenomenon strengthens the adhesion between the synthesized graphene and the MoS_2 layer.[29]

https://dx.doi.org/10.1021/acs.chemmater.0c00503
Chem. Mater. XXXX, XXX, XXX−XXX

The interfacial bonding was also examined at the interface by determining the Mo 3d XPS depth profile (Figure 2b). $3d_{5/2}$ (229.6 eV) and $3d_{3/2}$ (232.7 eV) peaks are evident for the TrGr; these peaks are consistent with the pure MoS_2 monolayer. The interaction between TrGr and the MoS_2 monolayer is weak, so the Mo 3d XPS is not shifted. The DiGr/MoS_2 (Figure S6) produces additional deconvoluted peaks at 228.9 eV (attributable to Mo−S) and 231.9 eV (attributable to Mo−C).[37] The results of the S 2p XPS analysis also support the interfacial bonding between DiGr and MoS_2, which is consistent with a previous study (Figure 2c).[38]

The Raman characteristics of graphene are sensitive to the surrounding materials. In particular, the 2D-peak is affected by the type of doping: blue-shifted by p-type dopants and red-shifted by n-type dopants.[39,40] Therefore, the 2D-peak shift can indicate the type of doping that the graphene has undergone. For TrGr/MoS_2, the 2D peak is blue-shifted due to the PMMA residues, which are strong p-type dopants to graphene (Figure 2d). For the DiGr/MoS_2 system, the 2D-peak is also blue-shifted by 18 cm^{-1}, despite the absence of a p-type dopant. This shift could be explained by the in-plane compression of graphene due to the 2.4% lattice mismatch between graphene (2.47 Å) and MoS_2 (3.20 Å).[41] Because of the lattice mismatch, the in-plane compression between two layers is applied during the growth of graphene. DiGr interacts strongly with the MoS_2 layer through interfacial adhesion bonding and it results in the blue-shift of the 2D-peak.[41] Our measured data indicates that the interaction between DiGr and the MoS_2 monolayer is enhanced by the chemical bonding and that this is the reason for the peak shifts in the XPS and Raman spectra.[42]

To assess the potential in device applications of the graphene/MoS_2 heterostructures obtained with our proposed method, we fabricated a MoS_2 field-effect transistor on a 300 nm SiO_2/Si substrate (Figure 3a). The MoS_2 monolayer was grown with CVD on the SiO_2/Si substrate, then TPN as the graphene growth precursor was spin-coated onto the MoS_2 monolayer. To pattern the graphene S/D electrodes, the precursor was selectively exposed to UV/ozone through a shadow mask. The TPN in the UV/ozone-exposed region adhered to the MoS_2 monolayer, so a graphene/MoS_2 vertical heterostructure was prepared on the SiO_2/Si substrate. During this process, TPN fully sublimated in the region where UV/ozone exposure was blocked, so no graphene formed in this region. As a result, the selective UV/ozone exposure yielded a patterned graphene structure in the MoS_2-FET device on the SiO_2/Si substrate. The patterned structure was examined with optical microscopy and two-dimensional Raman mapping (Figure S7). The two-dimensional $E_{2g}{}^1$ and 2D/G Raman mappings indicate that the MoS_2 monolayer is uniform over the whole area, including the channel region, and that the graphene/MoS_2 vertical heterostructure is present only in the DiGr S/D electrode regions. The single Raman spectrum clearly shows that the MoS_2 monolayer corresponds to the channel, and that the DiGr region corresponds to the S/D electrode region. The Raman characteristics of graphene (D peak ≈ 1352 cm^{-1}, G peak ≈ 1587 cm^{-1}, 2D peak ≈ 2687 cm^{-1}) are evident only in the S/D electrode regions. Thus, this approach efficiently facilitates the fabrication of MoS_2-FET devices by isolating the S/D electrodes without any interferences. We then used a Keithley 2636A instrument to measure the electrical characteristics of the device.

The measured transfer curves of the fabricated MoS_2-FET devices with DiGr S/D electrodes have the characteristics of a typical n-type transistor and a high on/off ratio ~10^7 (Figure 3b). From the transfer curves of the MoS_2-FET device, we obtained the field-effect carrier mobility, μ using the following equation

$$I_D = \frac{W}{2L} C\mu (V_G - V_T)^2 \quad (1)$$

where L [μm] is the channel length, I_D [μA] is the drain current, W [μm] is the channel width, C [F/cm^2] is the areal capacitance of the dielectric layer, V_G [V] is the gate voltage, and V_T [V] is the threshold voltage. In the saturation regime (V_{DS} = 500 mV), we obtained an average μ of 11.8 cm^2 V^{-1} s^{-1} for the 40 devices fabricated with our method (Figure 3c). However, in the case of the patterned transferred graphene (TrGr) electrodes, the MoS_2-FETs had an average μ of 3.9 cm^2 V^{-1} s^{-1}, which is less than one-third of the μ obtained with the DiGr electrodes. These results demonstrate that the DiGr S/D electrodes prepared with our method are appropriate for use in MoS_2-FETs.

To establish why the DiGr electrodes increase the μ of the fabricated MoS_2-FETs, we measured the contact resistance R_C, which is a critical factor determining device performance. The contact resistances, R_C of the DiGr and TrGr electrodes were calculated using the transfer-line method (TLM) for 100 ≤ L ≤ 250 μm (Figure S8). From the obtained TLM plots, each R_C was extracted from the L = 0 intersection of the following equation

$$R_{total} = 2R_c + \frac{L}{WC\mu}(V_G - V_T) = 2R_c + R_{ch} \quad (2)$$

where V_T [V] is the threshold voltage, R_{total} [Ω] is the total resistance, and R_{ch} [Ω] is the channel resistance. Normalization by R_CW was then performed, which shows that R_C is lower in DiGr electrodes than in TrGr electrodes (Figure 3d). Many previous studies have reported that the contact resistance is strongly influenced by various factors, especially the characteristics of the interface. In TrGr electrodes, the transfer process results in the non-uniform and unstable interface between MoS_2 and graphene (Figure S9), which contributes to an increase in R_C because it disrupts efficient charge injection and thereby degrades μ.[43] We surmise that the sharp interface obtained with our method results in MoS_2-FETs with improved electrical characteristics; in particular, the efficiency of charge injection from the DiGr S/D electrodes to the MoS_2 monolayer is enhanced.

The graphene synthesized on the MoS_2 monolayer using our method was expected to adhere strongly to each other due to the interfacial adhesion bonding induced by the UV/ozone treatment. First, the synthesized graphene/MoS_2 structure from the transfer method using the supporting polymer layer was transferred to a polyethylene terephthalate (PET) substrate for the bending stability test (Figure 3e). Then, the conductivities of MoS_2 were measured using the TrGr and DiGr electrodes, and the values obtained were 23.1 and 24.0 μS, respectively (Figure 3f). There was no significant difference when using the graphene electrodes from a conventional method or our method. However, as expected, a clear difference was observed under the repetitive cycle test at a bending radius of 10 mm (Figure 3g). The conductance change of the device using DiGr electrodes was decreased to ~0.8, which was higher than that of the device using TrGr

https://dx.doi.org/10.1021/acs.chemmater.0c00503
Chem. Mater. XXXX, XXX, XXX−XXX

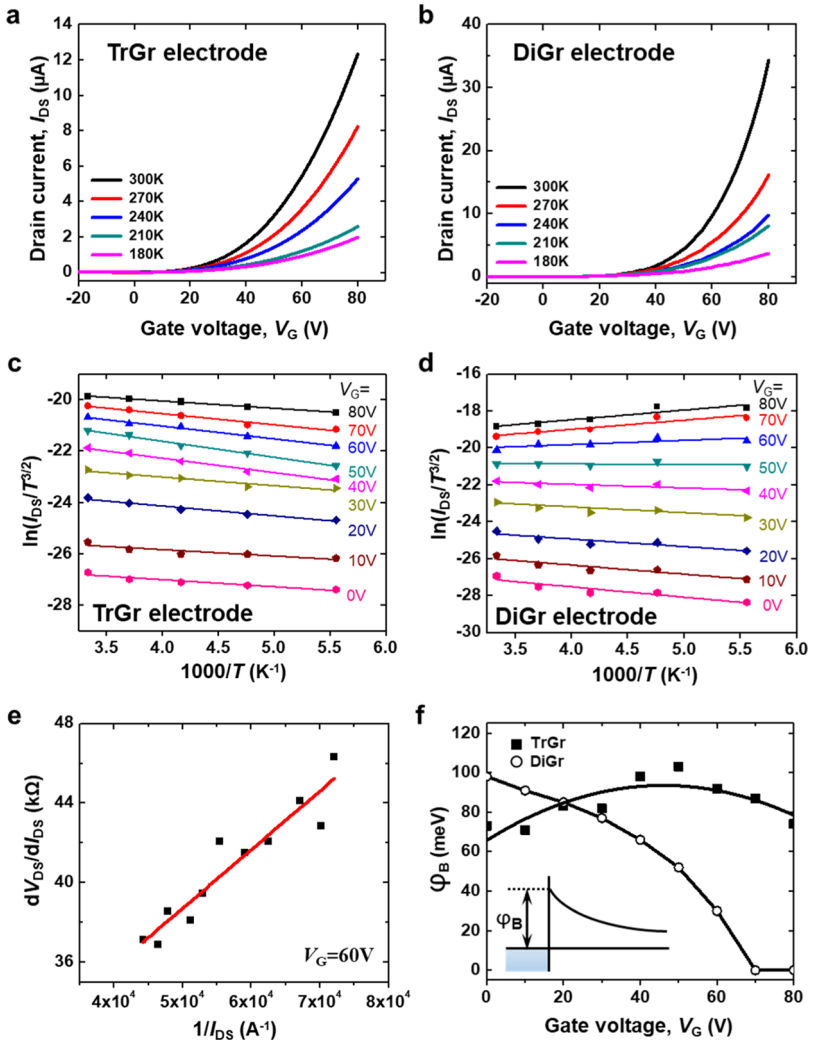

Figure 4. Temperature-dependent transfer characteristics and Schottky barrier height of the fabricated MoS_2-FETs. Electrical $I-V$ characteristics of the fabricated MoS_2-FETs using (a) TrGr and (b) DiGr as the S/D electrodes (V_{DS} = 500 meV). Arrhenius plots of monolayer MoS_2 using (c) TrGr and (d) DiGr as the S/D electrodes with different gate bias. (e) Plot of dV_{DS}/dI_{DS} as a function of $1/I_{DS}$ of MoS_2-FETs at V_G = 60 V for determining n. (f) Schottky barrier height, φ_B as a function of gate bias for CVD-grown MoS_2-FETs using TrGr and DiGr electrodes.

electrodes (~0.5). These results show that the weak interface between the conventionally transferred graphene and MoS_2 promoted further crack propagation. In contrast, DiGr was strongly bound to the MoS_2 monolayer, resulting in the improvement of the bending stability.

In addition to the reduction in the contact resistance of the MoS_2 FETs and the improvement of the bending stability obtained using a directly grown graphene electrode, this process has the additional advantage that it enables the formation of ohmic contact in the MoS_2-FETs. Note that the heights of the interfacial barriers between the electrodes and channel of devices based on 2D materials also affect their electrical characteristics. To investigate the barrier height of the contact between TrGr and MoS_2, the electrical properties of the devices fabricated using TrGr electrodes were determined at various temperatures (Figure 4a). It can be seen in this figure that the electrical current, I increases as the temperature increases because the charge transport in MoS_2 is governed by the hopping transport mechanism. The increase of current with temperature is due to the increase in the number of charge carriers at the elevated temperature that have sufficient thermal energy to overcome the activation energy.

Similarly, the electrical transport properties of the fabricated devices with DiGr electrodes were also determined at various temperatures (Figure 4b). The trend of temperature dependence is identical to that of the device with TrGr electrodes but the current level is much higher than in the devices with TrGr electrodes. To calculate φ_B from the obtained electrical $I-V$ results, we fitted the data using the following 2D thermal emission equation

$$I_{DS} = AT^{3/2} \exp\left(-\frac{q\varphi_B}{k_B T}\right)\left[\exp\left(\frac{qV_{DS}}{nk_B T}\right) - 1\right] \quad (3)$$

where I_{DS} [A] is the drain current, A is Richardson's constant, T [K] is the temperature, q is the electronic charge, k_B is the Boltzmann constant, V_{DS} [V] is the drain voltage, and n is the nonideal factor.[27,44] When $V_{DS} > 3k_B T$, eq 3 can be simplified to

$$\ln\left(\frac{I_{DS}}{T^{3/2}}\right) = -\frac{q\left(\varphi_B - \frac{V_{DS}}{n}\right)}{k_B T} + \ln(A) \quad (4)$$

https://dx.doi.org/10.1021/acs.chemmater.0c00503
Chem. Mater. XXXX, XXX, XXX−XXX

φ_B can be extracted from the slope of eq 4 in a plot of $\ln(I_{DS}/T^{3/2})$ versus $1000/T$, so we plotted the results obtained at different V_G for the devices with TrGr and DiGr electrodes (Figure 4c,d). To calculate φ_B from each slope value, we also need n, which can be calculated using the following equation

$$\frac{dV_{DS}}{dI_{DS}} = \frac{nk_BT}{q}\frac{1}{I_{DS}} + R_S \quad (5)$$

where R_s [Ω] is the series resistance of a Schottky diode. n can be determined from the slope of a plot of dV_{DS}/dI_{DS} versus $1/I_{DS}$; we found that n = 10.3, which is similar to the previously reported values[27] (Figure 4e).

Using these results, the φ_B values of the TrGr/MoS_2 and DiGr/MoS_2 contacts were calculated (Figure 4f). When no gate voltage is applied, the work function of the transferred graphene (~4.3 eV) is lower than that of the graphene obtained with our method (~4.5 eV) (Figure S10). Therefore, in the case of MoS_2, which has an electronic affinity of 4.1 eV, the Schottky barrier is lower when transferred graphene is used as the S/D electrodes. Interestingly, in the DiGr/MoS_2 contact system, the barrier height is reduced to 0 meV beyond V_G = 70 V, whereas for the TrGr/MoS_2 system, $60 \leq \varphi_B \leq 100$ meV. This result implies that the S/D electrodes consist of DiGr in the MoS_2 FET system; ideal ohmic contact is achieved at the interface between the MoS_2 and DiGr electrodes. In general, for an ideal metal contact with MoS_2, φ_B is determined by the difference between the work function of the metal and the electron affinity of the semiconductor. The work function of graphene can be modulated within 200 mV on a SiO_2 dielectric layer.[45,46] This modulation of the work function can align the energy at the interface and form an ohmic contact between MoS_2 and DiGr. However, in the TrGr/MoS_2 system, even though the work function of TrGr can be slightly modulated, the barrier height is also strongly influenced by various conditions such as organic contaminations (i.e., PMMA residues) and the characteristics of the interface.[27] Consequently, ohmic contact is not effectively achieved in the TrGr/MoS_2 system even at the high V_G.

4. CONCLUSIONS

In conclusion, we have developed a simple method for the synthesis of CVD graphene directly on MoS_2 monolayers using a surface-adhered solid carbon source. This method effectively produces a graphene/MoS_2 heterostructure with a sharp interface that facilitates charge injection and thereby improves the electrical characteristics of electronic devices based on 2D materials. The UV/ozone exposure induces interfacial adhesion between the MoS_2 monolayer and the TPN layer, so it can easily be converted directly to graphene in the presence of Cu vapor without any loss of TPN by sublimation at high growth temperatures. On SiO_2/Si substrates, we successfully fabricated MoS_2-FET devices with directly grown patterned S/D graphene electrodes using our suggested method. These devices were found to exhibit high μ because of the reduced R_C and ohmic contact between graphene and the MoS_2 monolayer. Also, their bending stability can be highly improved through interfacial adhesion bonding in the synthesized vertical heterostructure of graphene/MoS_2. Our proposed method provides a facile approach to the synthesis of graphene directly on TMDs including MoS_2 and thus to yield 2D-material-based ultrathin electronic devices that have excellent electrical characteristics.

■ ASSOCIATED CONTENT

Supporting Information

The Supporting Information is available free of charge at https://pubs.acs.org/doi/10.1021/acs.chemmater.0c00503.

CVD experimental condition, surface morphology of the substrates and Raman spectroscopy of pristine MoS_2, depth-profile XPS analysis, OM image, and two-dimensional Raman mapping image of the synthesized heterostructure, contact resistance measurement using transmission line method, high-resolution cross-sectional TEM image, and UPS curves (PDF)

■ AUTHOR INFORMATION

Corresponding Author

Kilwon Cho − *Department of Chemical Engineering and Center for Advanced Soft Electronics, Pohang University of Science and Technology, Pohang 37673, Korea;* orcid.org/0000-0003-0321-3629; Email: kwcho@postech.ac.kr

Authors

Eunho Lee − *Department of Chemical Engineering and Center for Advanced Soft Electronics, Pohang University of Science and Technology, Pohang 37673, Korea*

Seung Goo Lee − *Department of Chemistry, University of Ulsan, Ulsan 44610, Korea*

Wi Hyoung Lee − *Department of Organic and Nano System Engineering, Konkuk University, Seoul 05029, Korea;* orcid.org/0000-0002-2380-4517

Hyo Chan Lee − *Department of Chemical Engineering and Center for Advanced Soft Electronics, Pohang University of Science and Technology, Pohang 37673, Korea*

Nguyen Ngan Nguyen − *Department of Chemical Engineering and Center for Advanced Soft Electronics, Pohang University of Science and Technology, Pohang 37673, Korea*

Min Seok Yoo − *Department of Chemical Engineering and Center for Advanced Soft Electronics, Pohang University of Science and Technology, Pohang 37673, Korea*

Complete contact information is available at: https://pubs.acs.org/10.1021/acs.chemmater.0c00503

Notes

The authors declare no competing financial interest.

■ ACKNOWLEDGMENTS

This work was supported by a grant (code no. 2012M3A6A5055728) from the Center for Advanced Soft Electronics under the Global Frontier Research Program of the Ministry of Science and ICT, Korea.

■ REFERENCES

(1) Wilson, J. A.; Yoffe, A. D. The transition metal dichalcogenides discussion and interpretation of the observed optical, electrical and structural properties. *Adv. Phys.* **1969**, *18*, 193.

(2) Brar, V. W.; Koltonow, A. R.; Huang, J. New Discoveries and Opportunities from Two-Dimensional Materials. *ACS Photonics* **2017**, *4*, 407.

(3) Lee, Y.-H.; Zhang, X.-Q.; Zhang, W.; Chang, M.-T.; Lin, C.-T.; Chang, K.-D.; Yu, Y.-C.; Wang, J. T.-W.; Chang, C.-S.; Li, L.-J.; Lin, T.-W. Synthesis of Large-Area MoS_2 Atomic Layers with Chemical Vapor Deposition. *Adv. Mater.* **2012**, *24*, 2320.

(4) Lee, G.-H.; Yu, Y.-J.; Cui, X.; Petrone, N.; Lee, C.-H.; Choi, M. S.; Lee, D.-Y.; Lee, C.; Yoo, W. J.; Watanabe, K.; Taniguchi, T.; Nuckolls, C.; Kim, P.; Hone, J. Flexible and Transparent MoS_2 Field-

https://dx.doi.org/10.1021/acs.chemmater.0c00503
Chem. Mater. XXXX, XXX, XXX−XXX

Effect Transistors on Hexagonal Boron Nitride-Graphene Heterostructures. *ACS Nano* **2013**, *7*, 7931.
(5) Lim, H.; Yoon, S. I.; Kim, G.; Jang, A.-R.; Shin, H. S. Stacking of Two-Dimensional Materials in Lateral and Vertical Directions. *Chem. Mater.* **2014**, *26*, 4891.
(6) Das, S.; Gulotty, R.; Sumant, A. V.; Roelofs, A. All Two-Dimensional, Flexible, Transparent, and Thinnest Thin Film Transistor. *Nano Lett.* **2014**, *14*, 2861.
(7) Wei, D.; Liu, Y. Controllable Synthesis of Graphene and Its Applications. *Adv. Mater.* **2010**, *22*, 3225.
(8) Wang, D.-Y.; Huang, I.-S.; Ho, P.-H.; Li, S.-S.; Yeh, Y.-C.; Wang, D.-W.; Chen, W.-L.; Lee, Y.-Y.; Chang, Y.-M.; Chen, C.-C.; Liang, C.-T.; Chen, C.-W. Clean-lifting transfer of large-area residual-free graphene films. *Adv. Mater.* **2013**, *25*, 4521.
(9) Choi, W.; Choudhary, N.; Han, G. H.; Park, J.; Akinwande, D.; Lee, Y. H. Recent Development of Two-Dimensional Transition Metal Dichalcogenides and Their Applications. *Mater. Today* **2017**, *20*, 116.
(10) Li, X.; Cai, W.; An, J.; Kim, S.; Nah, J.; Yang, D.; Piner, R.; Velamakanni, A.; Jung, I.; Tutuc, E.; Banerjee, S. K.; Colombo, L.; Ruoff, R. S. Large-Area Synthesis of High-Quality and Uniform Graphene Films on Copper Foils. *Science* **2009**, *324*, 1312.
(11) Qiu, H.; Pan, L. J.; Yao, Z. N.; Li, J. J.; Shi, Y.; Wang, X. R. Electrical characterization of back-gated bi-layer MoS_2 field-effect transistors and the effect of ambient on their performances. *Appl. Phys. Lett.* **2012**, *100*, 123104.
(12) Liu, H.; Ye, P. D. $\hbox{MoS}_{2}$ Dual-Gate MOSFET With Atomic-Layer-Deposited $\hbox{Al}_{2}\hbox{O}_{3}$ as Top-Gate Dielectric. *IEEE Electron Device Lett.* **2012**, *33*, 546.
(13) Lee, K.; Kim, H.-Y.; Lotya, M.; Coleman, J. N.; Kim, G.-T.; Duesberg, G. S. Electrical Characteristics of Molybdenum Disulfide Flakes Produced by Liquid Exfoliation. *Adv. Mater.* **2011**, *23*, 4178.
(14) Lince, J. R.; Carré, D. J.; Fleischauer, P. D. Schottky-barrier formation on a covalent semiconductor without Fermi-level pinning: The metal-MoS_2(0001) interface. *Phys. Rev. B: Condens. Matter Mater. Phys.* **1987**, *36*, 1647.
(15) Kim, C.; Moon, I.; Lee, D.; Choi, M. S.; Ahmed, F.; Nam, S.; Cho, Y.; Shin, H.-J.; Park, S.; Yoo, W. J. Fermi Level Pinning at Electrical Metal Contacts of Monolayer Molybdenum Dichalcogenides. *ACS Nano* **2017**, *11*, 1588.
(16) Geim, A. K.; Grigorieva, I. V. Van der Waals heterostructures. *Nature* **2013**, *499*, 419.
(17) Allain, A.; Kang, J.; Banerjee, K.; Kis, A. Electrical contacts to two-dimensional semiconductors. *Nat. Mater.* **2015**, *14*, 1195.
(18) Gong, C.; Colombo, L.; Wallace, R. M.; Cho, K. The Unusual Mechanism of Partial Fermi Level Pinning at Metal-MoS_2 Interfaces. *Nano Lett.* **2014**, *14*, 1714.
(19) Leong, W. S.; Luo, X.; Li, Y.; Khoo, K. H.; Quek, S. Y.; Thong, J. T. L. Low Resistance Metal Contacts to MoS_2 Devices with Nickel-Etched-Graphene Electrodes. *ACS Nano* **2015**, *9*, 869.
(20) Chuang, H.-J.; Chamlagain, B.; Koehler, M.; Perera, M. M.; Yan, J.; Mandrus, D.; Tománek, D.; Zhou, Z. Low-Resistance 2D/2D Ohmic Contacts: A Universal Approach to High-Performance WSe_2, MoS_2, and $MoSe_2$ Transistors. *Nano Lett.* **2016**, *16*, 1896.
(21) Das, S.; Chen, H.-Y.; Penumatcha, A. V.; Appenzeller, J. High Performance Multilayer MoS_2 Transistors with Scandium Contacts. *Nano Lett.* **2013**, *13*, 100.
(22) Kappera, R.; Voiry, D.; Yalcin, S. E.; Branch, B.; Gupta, G.; Mohite, A. D.; Chhowalla, M. Phase-engineered low-resistance contacts for ultrathin MoS_2 transistors. *Nat. Mater.* **2014**, *13*, 1128.
(23) Gong, C.; Huang, C.; Miller, J.; Cheng, L.; Hao, Y.; Cobden, D.; Kim, J.; Ruoff, R. S.; Wallace, R. M.; Cho, K.; Xu, X.; Chabal, Y. J. Metal Contacts on Physical Vapor Deposited Monolayer MoS_2. *ACS Nano* **2013**, *7*, 11350.
(24) Liu, Y.; Wu, H.; Cheng, H.-C.; Yang, S.; Zhu, E.; He, Q.; Ding, M.; Li, D.; Guo, J.; Weiss, N. O.; Huang, Y.; Duan, X. Toward Barrier Free Contact to Molybdenum Disulfide Using Graphene Electrodes. *Nano Lett.* **2015**, *15*, 3030.
(25) Andleeb, S.; Eom, J.; Rauf Naz, N.; Singh, A. K. MoS_2 field-effect transistor with graphene contacts. *J. Mater. Chem. C* **2017**, *5*, 8308.
(26) Lee, Y. T.; Choi, K.; Lee, H. S.; Min, S.-W.; Jeon, P. J.; Hwang, D. K.; Choi, H. J.; Im, S. Graphene Versus Ohmic Metal as Source-Drain Electrode for MoS_2 Nanosheet Transistor Channel. *Small* **2014**, *10*, 2356.
(27) Yu, L.; Lee, Y.-H.; Ling, X.; Santos, E. J. G.; Shin, Y. C.; Lin, Y.; Dubey, M.; Kaxiras, E.; Kong, J.; Wang, H.; Palacios, T. Graphene/MoS_2 Hybrid Technology for Large-Scale Two-Dimensional Electronics. *Nano Lett.* **2014**, *14*, 3055.
(28) Zhou, J.; Lin, J.; Huang, X.; Zhou, Y.; Chen, Y.; Xia, J.; Wang, H.; Xie, Y.; Yu, H.; Lei, J.; Wu, D.; Liu, F.; Fu, Q.; Zeng, Q.; Hsu, C.-H.; Yang, C.; Lu, L.; Yu, T.; Shen, Z.; Lin, H.; Yakobson, B. I.; Liu, Q.; Suenaga, K.; Liu, G.; Liu, Z. A library of atomically thin metal chalcogenides. *Nature* **2018**, *556*, 355.
(29) Lee, E.; Lee, S. G.; Lee, H. C.; Jo, M.; Yoo, M. S.; Cho, K. Direct Growth of Highly Stable Patterned Graphene on Dielectric Insulators using a Surface-Adhered Solid Carbon Source. *Adv. Mater.* **2018**, *30*, 1706569.
(30) Ferrari, A. C.; Meyer, J. C.; Scardaci, V.; Casiraghi, C.; Lazzeri, M.; Mauri, F.; Piscanec, S.; Jiang, D.; Novoselov, K. S.; Roth, S.; Geim, A. K. Raman spectrum of graphene and graphene layers. *Phys. Rev. Lett.* **2006**, *97*, 187401.
(31) Pierucci, D.; Henck, H.; Avila, J.; Balan, A.; Naylor, C. H.; Patriarche, G.; Dappe, Y. J.; Silly, M. G.; Sirotti, F.; Johnson, A. T. C.; Asensio, M. C.; Ouerghi, A. Band Alignment and Minigaps in Monolayer MoS_2-Graphene van der Waals Heterostructures. *Nano Lett.* **2016**, *16*, 4054.
(32) Lee, E.; Lee, S. G.; Cho, K. Direct Growth of Substrate-Adhered Graphene on Flexible Polymer Substrates for Soft Electronics. *Chem. Mater.* **2019**, *31*, 4451.
(33) Fu, W.; Du, F. H.; Su, J.; Li, X. H.; Wei, X.; Ye, T. N.; Wang, K. X.; Chen, J. S. In situ catalytic growth of large-area multilayered graphene/MoS_2 heterostructures. *Sci. Rep.* **2014**, *4*, 4673.
(34) Lee, E.; Lee, H. C.; Jo, S. B.; Lee, H.; Lee, N.-S.; Park, C. G.; Lee, S. K.; Kim, H. H.; Bong, H.; Cho, K. Heterogeneous Solid Carbon Source-Assisted Growth of High-Quality Graphene via CVD at Low Temperatures. *Adv. Funct. Mater.* **2016**, *26*, 562.
(35) Liu, Q.; Cook, B.; Gong, M.; Gong, Y.; Ewing, D.; Casper, M.; Stramel, A.; Wu, J. Printable Transfer-Free and Wafer-Size MoS_2/Graphene van der Waals Heterostructures for High-Performance Photodetection. *ACS Appl. Mater. Interfaces* **2017**, *9*, 12728.
(36) Park, S.; Kim, S. Y.; Choi, Y.; Kim, M.; Shin, H.; Kim, J.; Choi, W. Interface Properties of Atomic-Layer-Deposited Al_2O_3 Thin Films on Ultraviolet/Ozone-Treated Multilayer MoS_2 Crystals. *ACS Appl. Mater. Interfaces* **2016**, *8*, 11189.
(37) Gu, L.; Ke, P.; Zou, Y.; Li, X.; Wang, A. Amorphous self-lubricant MoS_2-C sputtered coating with high hardness. *Appl. Surf. Sci.* **2015**, *331*, 66.
(38) Qie, L.; Chen, W. M.; Xiong, X. Q.; Hu, C. C.; Zou, F.; Hu, P.; Huang, Y. H. Sulfur-Doped Carbon with Enlarged Interlayer Distance as a High-Performance Anode Material for Sodium-Ion Batteries. *Adv. Sci.* **2015**, *2*, 1500195.
(39) Lee, S. K.; Yang, J. W.; Kim, H. H.; Jo, S. B.; Kang, B.; Bong, H.; Lee, H. C.; Lee, G.; Kim, K. S.; Cho, K. Inverse Transfer Method Using Polymers with Various Functional Groups for Controllable Graphene Doping. *ACS Nano* **2014**, *8*, 7968.
(40) Kim, H. H.; Yang, J. W.; Jo, S. B.; Kang, B.; Lee, S. K.; Bong, H.; Lee, G.; Kim, K. S.; Cho, K. Substrate-Induced Solvent Intercalation for Stable Graphene Doping. *ACS Nano* **2013**, *7*, 1155.
(41) Tang, Z.-K.; Zhang, Y.-N.; Zhang, D.-Y.; Lau, W.-M.; Liu, L.-M. The stability and electronic properties of novel three-dimensional graphene-MoS_2 hybrid structure. *Sci. Rep.* **2015**, *4*, 7007.
(42) Zhou, K.-G.; Withers, F.; Cao, Y.; Hu, S.; Yu, G.; Casiraghi, C. Raman Modes of MoS_2 Used as Fingerprint of van der Waals Interactions in 2-D Crystal-Based Heterostructures. *ACS Nano* **2014**, *8*, 9914.

https://dx.doi.org/10.1021/acs.chemmater.0c00503
Chem. Mater. XXXX, XXX, XXX−XXX

(43) Lu, Q.; Liu, Y.; Han, G.; Fang, C.; Shao, Y.; Zhang, J.; Hao, Y. Experimental investigation of the contact resistance of Graphene/MoS_2 interface treated with O_2 plasma. *Superlattices Microstruct.* **2018**, *114*, 421.
(44) Chen, J.-R.; Odenthal, P. M.; Swartz, A. G.; Floyd, G. C.; Wen, H.; Luo, K. Y.; Kawakami, R. K. Control of Schottky Barriers in Single Layer MoS_2 Transistors with Ferromagnetic Contacts. *Nano Lett.* **2013**, *13*, 3106.
(45) Yu, Y.-J.; Zhao, Y.; Ryu, S.; Brus, L. E.; Kim, K. S.; Kim, P. Tuning the Graphene Work Function by Electric Field Effect. *Nano Lett.* **2009**, *9*, 3430.
(46) Baik, S. S.; Im, S.; Choi, H. J. Work Function Tuning in Two-Dimensional MoS_2 Field-Effect-Transistors with Graphene and Titanium Source-Drain Contacts. *Sci. Rep.* **2017**, *7*, 45546.

https://dx.doi.org/10.1021/acs.chemmater.0c00503
Chem. Mater. XXXX, XXX, XXX−XXX